AIAA JOURNAL
Vol. 33, No. 4, April 1995

Predicting Stall and Post-Stall Behavior of Airfoils at Low Mach Numbers

Tuncer Cebeci,* Hamid Hefazi,† and Farzam Roknaldin‡
California State University, Long Beach, California 90840
and
Lawrence W. Carr§
NASA Ames Research Center, Moffett Field, California 94035

An interactive boundary-layer method, together with the e^n approach to the calculation of transition, is used to predict the stall and post-stall behavior of airfoils in incompressible and compressible flows at low freestream Mach numbers. Two separate inviscid methods—a panel method with compressibility corrections and a full potential method—are used to compute the external velocity distribution needed in the solution of the compressible boundary-layer equations. The turbulence model is based on the Cebeci-Smith algebraic eddy-viscosity formulation with improvements for strong pressure gradient effects. Comparison of calculated results with inviscid flow computed with a panel method indicate excellent agreement with experiment for a wide range of Reynolds numbers in incompressible flows. Comparison of calculated results obtained with inviscid flow computed with a full potential method also indicate excellent agreement with experiment for a wide range of angles of attack, including stall for compressible flows at low freestream Mach numbers. The study also shows that even though the compressibility corrections to the panel method are adequate at small-to-moderate angles of attack, they are not satisfactory at higher angles of attack, especially near stall.

I. Introduction

A PROBLEM of considerable interest in aerodynamics is the behavior of airfoils or helicopter blades at conventional wind-tunnel Reynolds numbers, which sometimes may be quite low. Even though in flight, Reynolds numbers are significantly higher than those in wind tunnels, and the behavior of the lifting bodies is not plagued with problems associated with small-scale wind-tunnel models, it is important that the calculation methods accurately predict the aerodynamic performance characteristics of the body so that flight conditions can be accurately simulated.

At high Reynolds numbers the performance characteristics of airfoils or helicopter blades can be predicted by methods based either on the solution of the Navier–Stokes equations or on a combination of inviscid and boundary-layer equations. In both approaches, the accuracy of the method depends on the numerical method, the turbulence model, and the method used to compute the location of the onset of transition. The differences between calculation methods for flight and wind-tunnel Reynolds numbers are mainly in the prediction of the transition location and in the modeling of the transition region. When the Reynolds number is high, the onset of transition occurs before or at the flow separation point, and the extent of the transition region is confined to a relatively small region. When transition occurs before laminar separation, it can be computed by correlation formulas such as those suggested by Michel[1] and Granville[2] or by the e^n method based on linear stability theory, as suggested by Smith[3] and van Ingen.[4] Several turbulence models, mostly developed for attached flows, can be used to model the transition region,[5] with models suggested by Dhawan and Narasimha[6] and by Chen and Thyson[7] being popular. Except at very high angles of attack where the flow corresponds to stall or post-stall conditions, these methods and models are often satisfactory in predicting airfoil flows, as discussed in Refs. 8 and 9. With decreasing Reynolds number (around chord Reynolds numbers of 5×10^5 to 1×10^5, however, rather large separation bubbles begin to appear on the airfoil; the onset of transition occurs inside the bubble and is separation induced. The importance of the turbulence model for the transition region increases and plays a larger role in the computational method. As a result the methods used to predict airfoil or blade characteristics at low Reynolds numbers must be modified to account for these phenomena that are either absent or not important at moderate wind-tunnel and high-Reynolds-number flows.[10–13]

Another important factor that must be considered in a calculation method is the role of the compressibility on stall angle at relatively low freestream Mach numbers. Although the Reynolds number on the airfoil may be small on a model at Mach numbers such as 0.15, with increasing Mach number, perhaps up to 0.5, the Reynolds number can vary by threefold. The behavior of the flow, the change of the length of the separation bubble, and the movement of the transition location within the separation bubble must be predicted accurately to calculate the stall angle at each Mach number.

This paper presents an efficient and accurate method for calculating the stall and post-stall behavior of airfoils at low and high Reynolds numbers. The method is based on the solution of inviscid and boundary-layer equations with the onset of transition computed with the e^n method based on linear stability theory. The method is developed for incompressible and compressible flows at low freestream Mach numbers. For incompressible flows, the inviscid method is calculated with a panel method.[14] For compressible flows, the inviscid flow is calculated 1) by introducing compressibility corrections to the panel method and 2) by using a full potential method.[15]

The following section describes the calculation method and is followed by Sec. III, which presents the results for several airfoils in incompressible and compressible flows. The paper ends with a summary of the more important conclusions.

II. Calculation Method

A. Interactive Boundary-Layer Method

With inviscid flow solutions given either by a panel method or a full-potential method, the viscous flow solutions are obtained from the compressible boundary-layer equations in which the turbulence

Received Oct. 1, 1993; revision received May 5, 1994; accepted for publication May 6, 1994.

*Professor and Chair, Aerospace Engineering Department. Fellow AIAA.
†Professor, Aerospace Engineering Department. Senior Member AIAA.
‡Graduate Student, Aerospace Engineering Department.
§Research Scientist and Group Leader, Unsteady Viscous Flows, Aeroflightdynamics Directorate, U.S. Army ATCOM, and Fluid Mechanics Laboratory Branch.

model is given by the algebraic eddy viscosity ε_m and turbulent Prandtl number Pr_t formulation of Cebeci and Smith[5]:

$$\frac{\partial}{\partial x}(\rho u) + \frac{\partial}{\partial y}(\overline{\rho v}) = 0 \tag{1}$$

$$\rho u\frac{\partial u}{\partial x} + \overline{\rho v}\frac{\partial u}{\partial y} = \rho_e u_e \frac{\mathrm{d}u_e}{\mathrm{d}x} + \frac{\partial}{\partial y}\left[(\mu + \rho\varepsilon_m)\frac{\partial u}{\partial y}\right] \tag{2}$$

$$\rho u\frac{\partial H}{\partial x} + \overline{\rho v}\frac{\partial H}{\partial y} = \frac{\partial}{\partial y}\left[\left(k + c_p\rho\frac{\varepsilon_m}{Pr_t}\right)\frac{\partial T}{\partial y} + u(\mu + \rho\varepsilon_m)\frac{\partial u}{\partial y}\right] \tag{3}$$

where $\overline{\rho v} = \rho v + \overline{\rho' v'}$. In the absence of mass transfer, the boundary conditions for an adiabatic surface are

$$y = 0, \qquad u = v = 0, \qquad \frac{\partial H}{\partial y} = 0 \tag{4a}$$

$$y \to \infty, \qquad u \to u_e(x), \qquad H \to H_e \tag{4b}$$

and in the wake, where a dividing line at $y = 0$ is required to separate the upper and lower parts of the inviscid flow, and in the absence of the normal pressure gradient, they are

$$y \to \pm\infty, \qquad u \to u_e(x), \qquad H \to H_e; \qquad y = 0, \qquad v = 0 \tag{5}$$

To perform the calculations for flows with separation, an inverse procedure is used, and the external velocity is computed as part of the solution. According to the formulation discussed in Ref. 8, the edge boundary condition is written as

$$u_e(x) = u_e^0(x) + \delta u_e(x) \tag{6a}$$

where $\delta u_e(x)$ is computed from the Hilbert integral

$$\delta u_e(x) = \frac{1}{\pi}\int_{x_a}^{x_b}\frac{\mathrm{d}}{\mathrm{d}\sigma}(u_e\delta^*)\frac{\mathrm{d}\sigma}{x - \sigma} \tag{6b}$$

B. Turbulence Model

The turbulence model used to represent the flow on the airfoil is expressed in terms of the Cebeci and Smith eddy-viscosity formulation,[5]

$$\varepsilon_m = \begin{cases} (\varepsilon_m)_i = \left\{0.4y\left[1 - \exp\left(\dfrac{-y}{A}\right)\right]\right\}^2\left|\dfrac{\partial u}{\partial y}\right|\gamma_{\mathrm{tr}}, & 0 \le y \le y_c \quad (7a) \\ (\varepsilon_m)_0 = \alpha\left|\displaystyle\int_0^\infty (u_e - u)\,\mathrm{d}y\right|\gamma_{\mathrm{tr}}\gamma, & y_c \le y \le \delta \quad (7b) \end{cases}$$

The condition used to define y_c is the continuity of the eddy viscosity, and so Eq. (7a) is applied from the wall outward (inner region) until its value is equal to that given for the outer region by Eq. (7b). The parameters A and γ are defined by

$$A = 26\nu u_\tau^{-1}(\rho/\rho_w)^{\frac{1}{2}}, \qquad u_\tau = \left(\frac{\tau}{\rho}\right)_{\max}^{\frac{1}{2}}, \qquad \gamma = \frac{1}{1 + 5.5(y/\delta)^6} \tag{8a}$$

and α, as discussed in Ref. 16,

$$\alpha = 0.0168\Big/\left\{\left[1 - \beta\left(\frac{\partial u}{\partial x}\right)\Big/\left(\frac{\partial u}{\partial y}\right)\right]^{1.5}\right\} \tag{8b}$$

where β [with R_t denoting the ratio of wall shear stress to maximum Reynolds stress, $\tau_w/(-\overline{\rho u' v'})_m$,] is given by

$$\beta = \begin{cases} \dfrac{6}{1 + 2R_t(2 - R_t)} & R_t < 1.0 \\ \dfrac{1 + R_t}{R_t} & R_t \ge 1.0 \end{cases} \tag{9}$$

For $\tau_w < 0$, R_t is set equal to zero.

The expression γ_{tr} represents the transition region and is given by

$$\gamma_{\mathrm{tr}} = 1 - \exp\left[-G(x - x_{\mathrm{tr}})\int_{x_{\mathrm{tr}}}^{x}\frac{\mathrm{d}x}{u_e}\right] \tag{10a}$$

Here x_{tr} is the location of the beginning of transition, and G is defined by

$$G = \frac{3}{C^2}\frac{u_e^3}{\nu_e^2}R_{x_{\mathrm{tr}}}^{-1.34} \tag{10b}$$

where C is 60 for attached flows, and the transition Reynolds number $R_{x_{\mathrm{tr}}} = (u_e x/\nu_e)_{\mathrm{tr}}$.

The corresponding eddy-viscosity expressions in the wake are

$$\varepsilon_m = (\varepsilon_m)_w + [(\varepsilon_m)_{t.e} - (\varepsilon_m)_w]\exp\left[\frac{(x - x_0)}{20\delta}\right] \tag{11}$$

where $(\varepsilon_m)_{t.e.}$ is the eddy viscosity at the trailing edge computed from Eqs. (7), and $(\varepsilon_m)_w$ is the eddy viscosity in the far wake given by the larger of

$$(\varepsilon_m)_w^\ell = 0.064\int_{-\infty}^{y_{\min}}(u_e - u)\,\mathrm{d}y \tag{12a}$$

and

$$(\varepsilon_m)_w^u = 0.064\int_{y_{\min}}^{\infty}(u_e - u)\,\mathrm{d}y \tag{12b}$$

The calculation of airfoils at chord Reynolds numbers less than 10^6 requires changes to the turbulence model given by Eqs. (7). According to the γ_{tr} model used in the Cebeci–Smith (CS) model and given by Eqs. (10a) and (10b), the extent of the transition region $R_{\Delta x}$ is related to the transition Reynolds number $R_{x_{\mathrm{tr}}}$ by

$$R_{\Delta x} = CR_{x_{\mathrm{tr}}}^{2/3} \tag{13}$$

which shows that $R_{\Delta x}$ increases with decreasing $R_{x_{\mathrm{tr}}}$. This expression was obtained from data based on attached flows and is not applicable to flows with separation. Experiments show that the extent of the separation bubble and the location of the onset of transition depend upon the Reynolds number. At high Reynolds numbers, transition usually corresponds to the location of separation, and the length of the bubble is relatively short. At low Reynolds numbers, transition can occur inside the bubble and can strongly influence the nature of flow. To take account of the corresponding effects, a correlation formula was developed in Ref. 13; the parameter C in Eq. (10b) was expressed in terms of $R_{x_{\mathrm{tr}}}$ by

$$C^2 = 213\left(\log R_{x_{\mathrm{tr}}} - 4.7323\right) \tag{14}$$

in the Reynolds number range from $R_c = 2.4 \times 10^5$ to 2×10^6.

C. Transition Method

The onset of transition is calculated from the e^n method, which is based on the linear stability theory. Since the study conducted here is for low Mach numbers, the compressibility effect on transition was neglected, and the incompressible form of the Orr-Sommerfeld equation

$$\phi^{iv} - 2\alpha^2\phi'' + \alpha^4\phi - iR(\alpha\bar{u} - \omega)(\phi'' - \alpha^2\phi) + iR\alpha\bar{u}''\phi = 0 \tag{15}$$

was solved for given velocity profiles $\bar{u}$ and $\bar{u}''$ and for a set of specified dimensional frequencies ω^* at x_0 to obtain the amplification

rates so that for each frequency the value of n can be obtained from the integral

$$n = -\int_{x_0}^{x} \alpha_i \, dx \tag{16}$$

Transition is obtained from the resulting curves corresponding to the maximum amplification factor by assuming n to be 9.

D. Compressibility Corrections to the Panel Method

The compressibility corrections used in the panel method depend upon the linearized form of the compressible velocity potential equation and are based on the assumption of small perturbations and thin airfoils. A simple correction formula used here is the Karman-Tsien formula that uses the tangent gas approximation to simplify the compressible potential-flow equations. According to this formula, the effect of Mach number on the pressure coefficient is estimated from

$$C_p = \frac{C_{p_i}}{\tilde{\beta} + \left[M_\infty^2/(1+\tilde{\beta})\right]\left(C_{p_i}/2\right)} \tag{17}$$

and the corresponding velocities are computed from

$$\frac{V}{V_\infty} = \frac{(1-\lambda)(V/V_\infty)_i}{1-\lambda(V/V_\infty)_i^2} \tag{18a}$$

where C_{p_i} denotes the incompressible pressure coefficient and

$$\lambda = \frac{M_\infty^2}{1+\tilde{\beta}^2}, \qquad \tilde{\beta} = \sqrt{1-M_\infty^2} \tag{18b}$$

E. Solution Procedure

A brief description of the solution procedure used in this method is as follows. The panel or the full-potential method provides an external velocity distribution and identifies the stagnation point. The interactive boundary-layer method leads to solutions on the upper and lower surfaces from the stagnation point through the regions of laminar, transitional, and turbulent flow to the trailing edge. With the upper and lower surface velocity profiles computed at the trailing edge, the calculations are extended into the wake. As a consequence of the aforementioned, a blowing velocity defined by

$$v_n = \frac{d}{dx}(u_e \delta^*) \tag{19}$$

is available on the airfoil and in the wake and is used to obtain a new distribution of external velocity $u_{ei}(x)$ from the inviscid method. As before, the boundary-layer solutions on the upper and lower surfaces of the airfoil and in the wake are obtained with the Hilbert integral. This sequence of calculations is repeated for the whole flowfield until convergence is achieved.

In all cases except at high angles of attack, the onset of transition is obtained with the e^n method. At higher angles of attack, the onset of transition location was assumed to occur at the pressure peak and was not computed.

III. Results and Discussion

The results are presented in two sections. In Sec. III.A the inviscid flow was computed by using the panel method, and the results are presented for several airfoils in incompressible flows to show the accuracy of the method for predicting the stall and post-stall behavior of airfoils at low and high Reynolds numbers. Since extensive regions of separation bubbles can occur on airfoils at low Reynolds numbers, studies are also conducted to investigate the extent of the separation bubble and the location of onset of transition on the airfoils, as well as the reduction of stall angle due to Reynolds number effects. In Sec. III.B results are presented for several airfoils measured in Ref. 17 to investigate the compressibility effect on stall angle. For this purpose the inviscid flow was computed by using either the panel method with compressibility corrections or with the full-potential method. The studies were conducted at moderate Reynolds numbers.

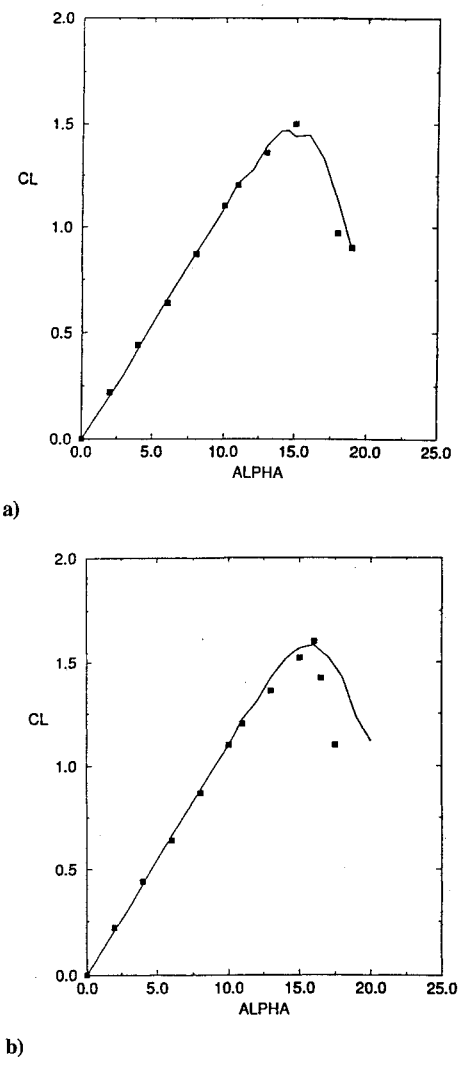

Fig. 1 Effect of Reynolds number on the lift coefficient of a NACA 0012 airfoil: a) $R_c = 3 \times 10^6$ and b) $R_c = 6 \times 10^6$.

A. Incompressible Flows

The calculations were first performed for three airfoils, the NACA 0012, NACA 23012, and Sikorsky SSC-A09, at high Reynolds numbers where the transition region is negligible (see Ref. 18). At low-to-moderate angles of attack, the onset of transition is calculated by using the e^n method. At higher angles of attack, the onset of transition was assumed to correspond to laminar separation, which occurs very close to the pressure peak. The results, however, are presented here for the NACA 0012 airfoil only. For additional results, see Ref. 18.

Figure 1 shows a comparison between calculated and measured lift coefficients for the NACA 0012 airfoil at chord Reynolds numbers corresponding to 3×10^6 and 6×10^6. As can be seen, in accord with the measurements, the calculation method is able to compute C_ℓ for all angles of attack and satisfactorily account for the Reynolds number effect.

It is useful to examine the extent of flow separation on the airfoil and the variation of the displacement thickness on the airfoil and in the wake at high angles of attack. Figures 2 and 3 show the variation of local skin coefficient and displacement thickness distribution on the NACA 0012 airfoil at $R_c = 3 \times 10^6$. As can be seen from Fig. 2, flow separation occurs for $\alpha > 10$ deg, and its extent increases with increasing angle of attack. At an incidence angle of attack $\alpha = 18$ deg, the flow separation on the airfoil is 60% of the chord length.

The variations of dimensionless displacement thickness δ^*/c along the airfoil and wake of the airfoil shown in Fig. 3 indicate that, as expected, displacement thickness increases along the airfoil, becoming maximum at the trailing edge, and decreases in the wake. Its magnitude increases with increase in angle of attack. For $\alpha = 10$ deg, δ^*/c at the trailing edge is around 2% of the chord, becoming

Table 1 Laminar separation (LS), transition $(x/c)_{tr}$, and turbulent reattachment (TR) locations on the Eppler airfoil, $R_c = 3 \times 10^5$

	Experiment			Calculated	
α, deg	LS	TR	$(x/c)_{tr}$	LS	TR
0	0.48	0.69	0.653	0.515	0.72
4	0.40	0.58	0.541	0.42	0.60

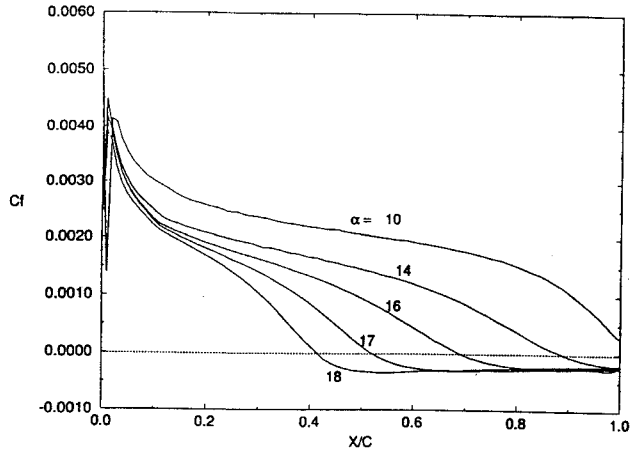

Fig. 2 Variation of local skin-friction coefficient on the NACA 0012 airfoil for $R_c = 3 \times 10^6$.

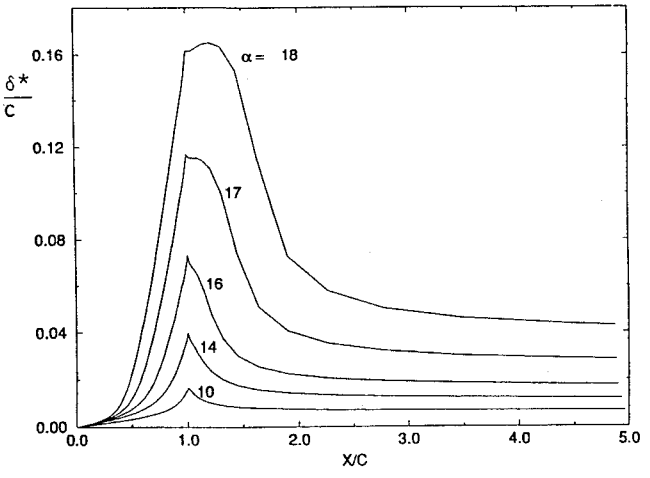

Fig. 3 Variation of dimensionless displacement thickness distribution δ^*/c on the NACA 0012 airfoil and its wake for $R_c = 3 \times 10^6$.

4% at $\alpha = 14$ deg and 7% at $\alpha = 16$ deg, which is the stall angle for this airfoil at this Reynolds number. With increase in angle of attack, the trailing-edge displacement thickness increases significantly, becoming 12% of the chord at $\alpha = 17$ deg and 16% at $\alpha = 18$ deg. However, what is quite interesting, aside from this rather sharp increase in displacement thickness, is the behavior of the maximum value of the displacement thickness: whereas for angles of attack up to and including stall angle, $\alpha = 16$ deg, its maximum is at the trailing edge, at higher angles of attack corresponding to post stall, its maximum value is after the trailing edge.

Figure 4 shows the variation of the lift coefficient of the NACA 0012 airfoil for a chord Reynolds number of 2×10^5 together with the results obtained at $R_c = 3 \times 10^6$. As can be seen, the Reynolds number has a significant effect, not only on the magnitude of the maximum lift coefficient, but also on the stall angle. With this change in Reynolds number, the $(C_\ell)_{max}$ is reduced from a value of 1.5 to a value slightly over 1. The corresponding reduction in angle of attack is from 16 to around 11 deg.

Table 1 and Figs. 5–7 show a sample of the results for an Eppler airfoil at a chord Reynolds number of 3×10^5. These recent results also reported in Ref. 19 were obtained with the present calculation

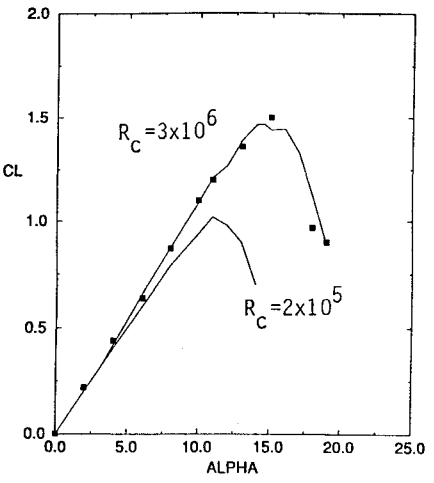

Fig. 4 Variation of lift coefficient of the NACA 0012 airfoil at two Reynolds numbers.

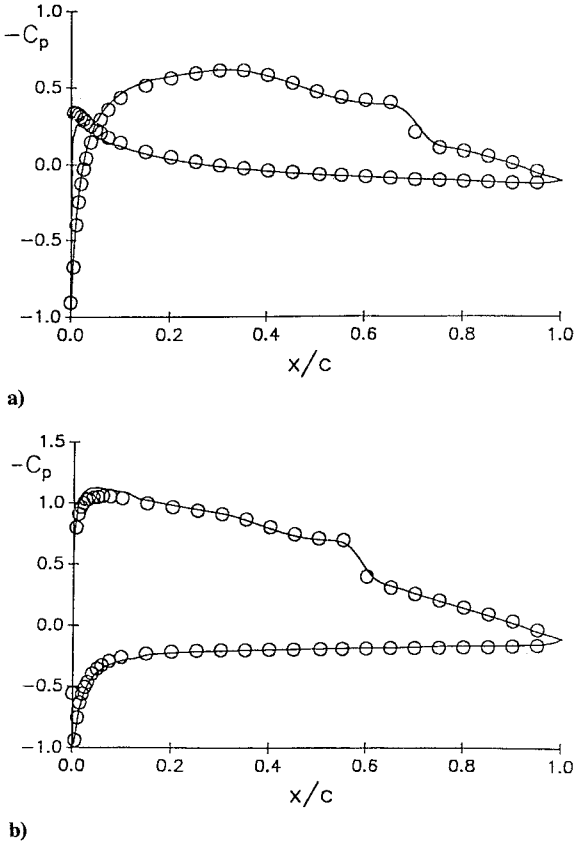

Fig. 5 Comparison of calculated (solid lines) and measured (symbols) pressure coefficient distributions for a) $\alpha = 0$ deg and b) $\alpha = 4$ deg at $R_c = 3 \times 10^5$.

method for a wide range of angles of attack at Reynolds numbers corresponding to 2×10^5 and 3×10^5. The experimental data were obtained by McGhee et al.[20] in the Langley Low-Turbulence Pressure Tunnel (LTPT). The tests were conducted at Mach numbers from 0.03 to 0.13 and at chord Reynolds numbers from 6×10^4 to 4.6×10^5. Lift and pitching-moment data were obtained from airfoil surface pressure measurements and drag data from wake surveys. Oil flow visualization was used to determine laminar separation and turbulent reattachment locations.

Table 1 shows the laminar separation (LS), onset of transition $(x/c)_{tr}$, and turbulent reattachment (TR) locations on the upper surface of the Eppler airfoil for angles of attack corresponding to $\alpha = 0$ and 4 deg. As can be seen, the onset of transition occurs inside the separation bubble, and the airfoil has an extensive separation bubble that decreases in size with increase in α.

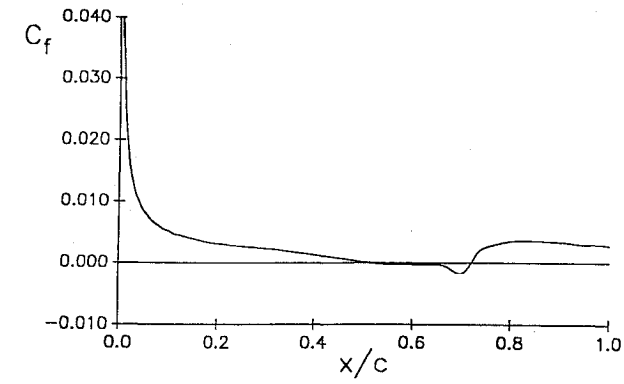

a)

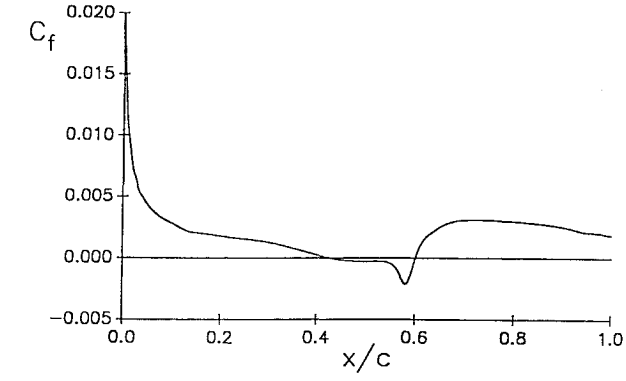

b)

Fig. 6 Variation of the calculated local skin-friction coefficient on the airfoil for a) α = 0 deg and b) α = 4 deg for $R_c = 3 \times 10^5$.

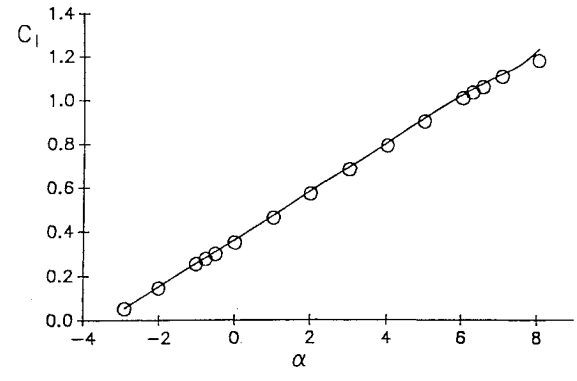

a)

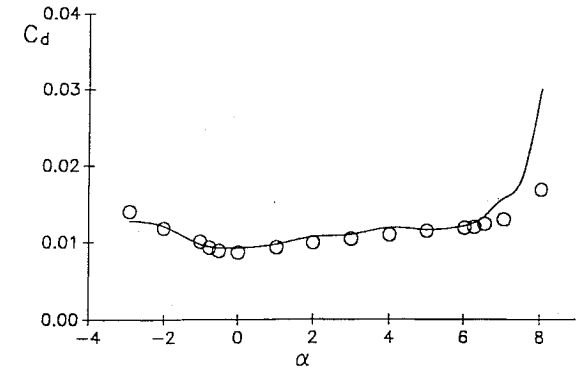

b)

Fig. 7 Comparison of calculated (solid lines) and measured (symbols) a) lift and b) total drag coefficients for the Eppler airfoil at $R_c = 3 \times 10^5$.

Figure 5 shows a comparison between the calculated and measured pressure coefficient distributions for $\alpha = 0$ and 4 deg, and Fig. 6 shows the variation of the local skin-friction coefficient c_f along at the airfoil. The comparison between calculations and experiment is excellent, and the calculation method accounts well for the relatively large separation bubble at both angles of attack. Figure 7 shows the same good agreement in lift and drag coefficients for a range of angles of attack.

B. Compressible Flows at Low Mach Numbers and at High Reynolds Numbers

The effect of compressibility on stall at low freestream Mach numbers and at high Reynolds numbers was investigated for four airfoils; the experimental data were taken at NASA Ames by Carr et al.[17] A comparison of calculated results with experimental data are given next for a sample of airfoils. For additional results, see Ref. 18.

Before examining the results, it is useful to describe the procedure employed for performing the wake calculations in the interactive scheme. The viscous wake calculations require a streamline issuing from the trailing edge of the airfoil. The computation of the location of this streamline is relatively simple if conformal mapping methods are used to determine the velocity field. In this case, the stream function ψ is usually known, and because the airfoil surface is represented by $\psi(x, y) = \text{const}$, the calculation of the wake streamline amounts to tracing the curve after it leaves the airfoil. When the flowfield is computed by a panel method or by a full-potential method, however, the results are known only at discrete points in the field in terms of the velocity components. In this case, the wake streamline can be determined from the numerical integration of

$$\frac{dy}{dx} = \frac{v}{u} \tag{20}$$

aft of the trailing edge with known initial conditions. This is the procedure we used for the panel method; for the full-potential method, the discrete points in the wake were arbitrarily used to represent the streamline needed in the viscous wake calculations. As shall be shown later, this procedure is not a good one and needs to be improved, since the solutions near the trailing edge exhibits an irregular behavior.

Figures 8–10 show the results for the NACA 0012 airfoil at a Mach number of 0.3 and for a chord Reynolds number of 4×10^6. This airfoil was the standard helicopter airfoil during the early period of development of helicopters and has become a benchmark for comparison of computation and experiment.

Figures 8 and 9 compare the calculated pressure coefficient distributions with measurements for two angles of attack corresponding to $\alpha = 13$ and 13.5 deg. The results in Fig. 8 correspond to calculations employing the panel method with compressibility corrections, and Fig. 9 shows the results from employing the full-potential method. As can be seen, the calculations (using the same boundary-layer method) produce results in which the full-potential results are in better agreement than those obtained with the panel method with compressibility corrections. Such a comparison is important because it is generally believed that the compressibility corrections are often satisfactory to account for the compressibility effects at low Mach numbers.

Figure 10 shows a comparison between the calculated lift coefficients with experimental data. Again, the solutions employing the full-potential method produce results that agree well with the measurements. Although to some extent the compressibility corrections to the panel method improve the agreement with experimental data, panel method solutions are not as accurate as those predicted with the full-potential method; the $(C_\ell)_{max}$ is underpredicted by a significant amount, and lift values are not even very accurate before stall. It is useful to note that for $M_\infty = 0$, the $(C_\ell)_{max}$ for this airfoil is close to 1.5 at $R_c = 3 \times 10^6$ and is close to 1.6 at $R_c = 6 \times 10^6$. According to Fig. 10, at a relatively low Mach number of 0.3, the $(C_\ell)_{max}$ is reduced to around 1.4 at $R_c = 4 \times 10^6$.

Figures 11–13 show the results for the AMES 01 airfoil at a Mach number of 0.3 and at a chord Reynolds number of 3.84×10^6. This airfoil was designed for helicopter applications, using a numerical optimization approach.[21] This multipoint optimization combined high lift at moderate subsonic Mach numbers (on the "retreating"

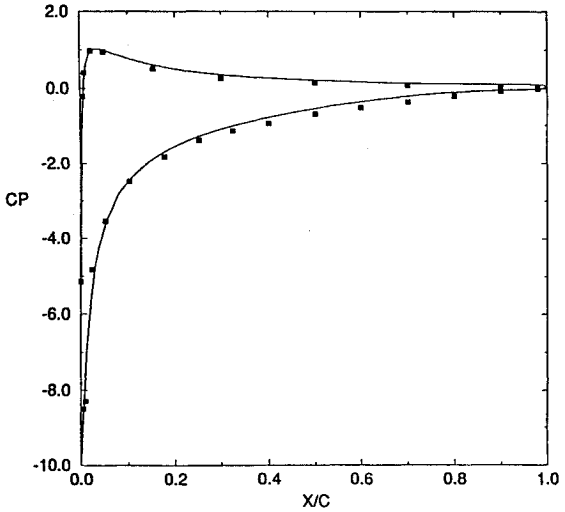

a)

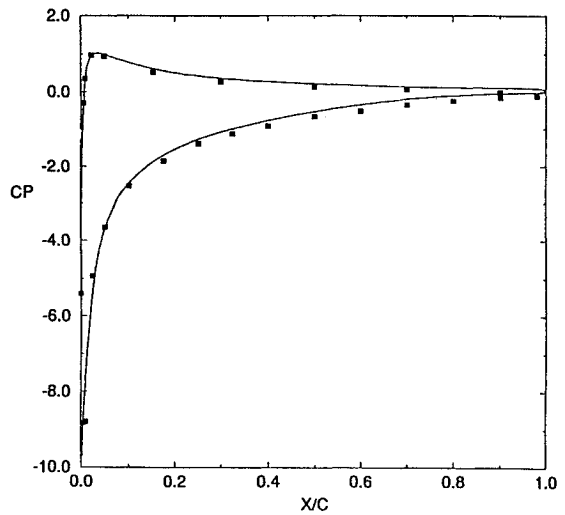

b)

Fig. 8 Comparison of calculated (solid lines) and measured (symbols) pressure coefficient distributions with the modified panel method for the NACA 0012 airfoil at $M_\infty = 0.3$ and $R_c = 4 \times 10^6$: a) $\alpha = 13$ deg and b) 13.5 deg.

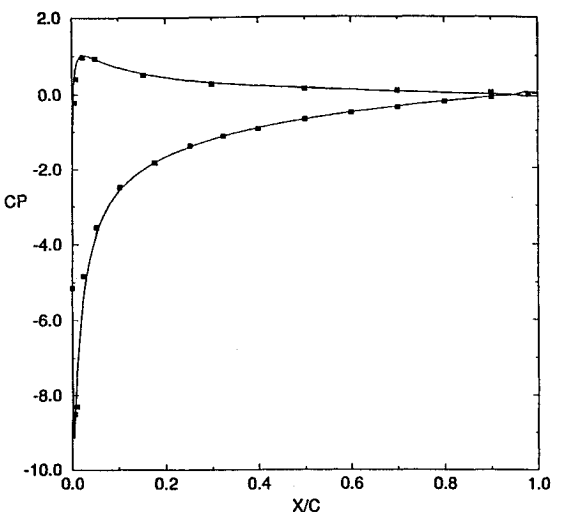

a)

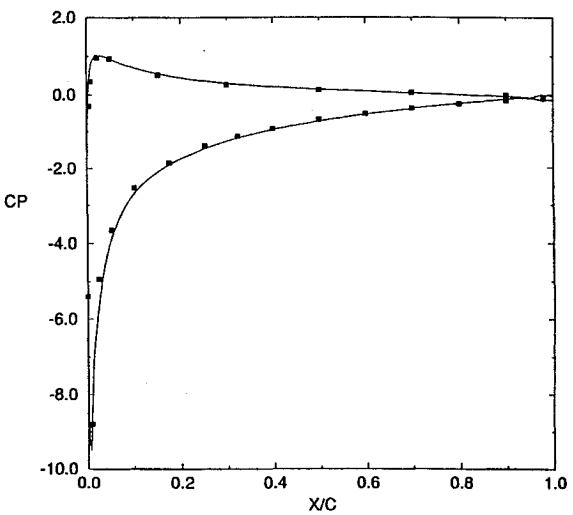

b)

Fig. 9 Comparison of calculated (solid lines) and measured (symbols) pressure coefficient distributions with the full-potential method for the NACA 0012 airfoil at $M_\infty = 0.3$ and $R_c = 4 \times 10^6$: a) $\alpha = 13$ deg and b) 13.5 deg.

blade of the helicopter rotor) with restraints placed on shock-induced drag divergence at transonic Mach numbers (on the "advancing" blade).

Figures 11 and 12 show comparisons between calculated and measured pressure coefficient distributions at $\alpha = 13.5$ deg, obtained with the full-potential method, and with the panel method employing compressibility corrections, respectively. For additional angles of attack, see Ref. 18. The variation of calculated and measured lift coefficient with angle of attack is shown in Fig. 13. Consistent with the results for the NACA 0012 airfoil, the calculated results with the modified panel method are not as accurate as those computed with the full-potential method. Again the discrepancy becomes more pronounced at higher angles of attack. The predicted lift coefficients with the full-potential method are in good agreement with measurements for all angles of attack, in contrast to the predicted lift coefficients with the modified panel method, even at moderate angles of attack.

Figures 14–16 show similar results for the NLR-1 airfoil at a Mach number of 0.3 and at a chord Reynolds number of 3.91×10^6. This airfoil is also based on the "peakey" airfoil concept developed by Wortmann,[22] combined with an inverse camber built into the trailing-edge region of the airfoil to reduce the pitching moment.[23]

Figures 14 and 15 show comparisons between calculated and measured pressure coefficient distributions at $\alpha = 12$ deg, and Fig. 16

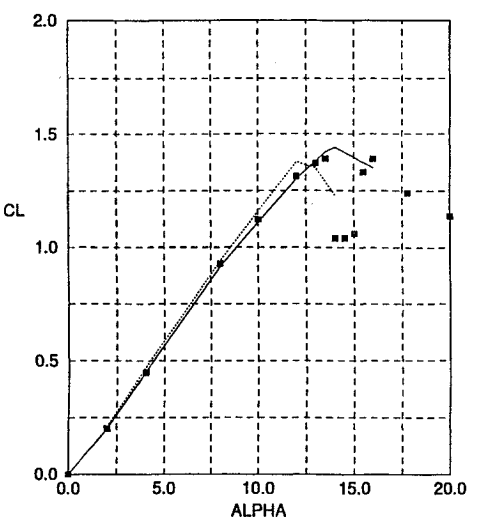

Fig. 10 Comparison of calculated and measured lift coefficients for the NACA 0012 airfoil at $M_\infty = 0.3$ and $R_c = 4 \times 10^6$. Solid lines denote the results with the full-potential method and dashed lines those with the modified panel method.

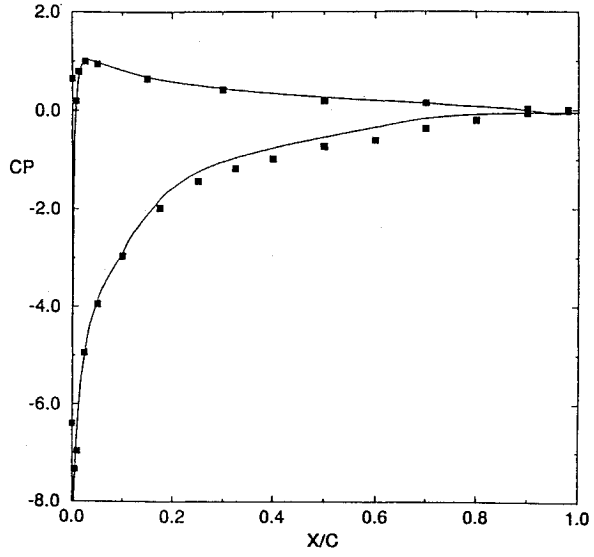

Fig. 11 Comparison of calculated (solid lines) and measured (symbols) pressure coefficient distributions with the modified panel method for the Ames 01 airfoil at $M_\infty = 0.3, R_c = 3.84 \times 10^6$, and $\alpha = 13.5$ deg.

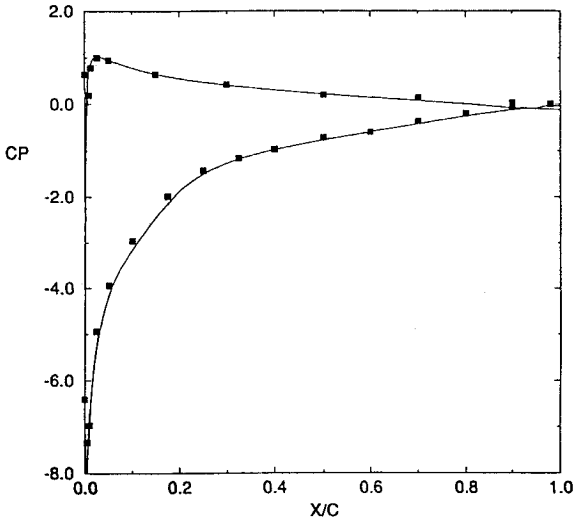

Fig. 12 Comparison of calculated (solid lines) and measured (symbols) pressure coefficient distributions with the full-potential method for the AMES 01 airfoil at $M_\infty = 0.3, R_c = 3.84 \times 10^6$, and $\alpha = 13.5$ deg.

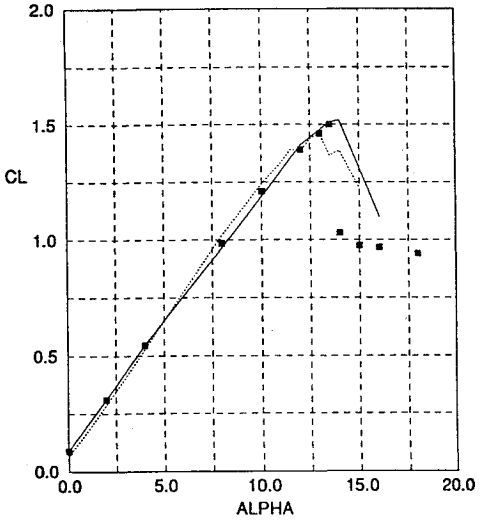

Fig. 13 Comparison of calculated and measured lift coefficients for the AMES 01 airfoil at $M_\infty = 0.3$ and $R_c = 3.84 \times 10^6$. Solid lines denote the results with the full-potential method and dashed lines those with the modified panel method.

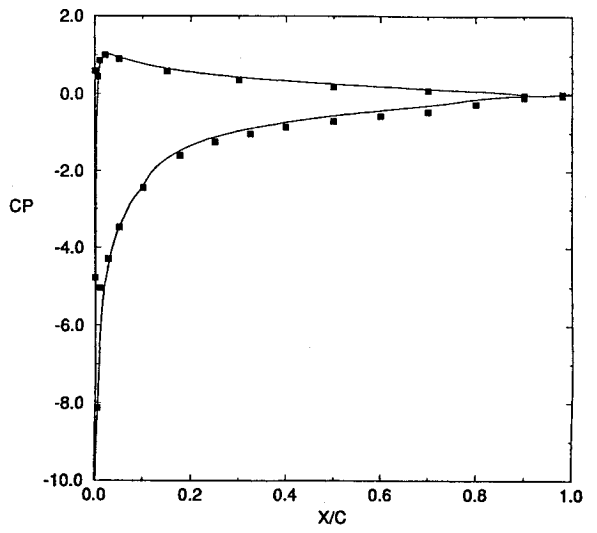

Fig. 14 Comparison of calculated (solid lines) and measured (symbols) pressure coefficient distributions with the modified panel method for the NLR-1 airfoil at $M_\infty = 0.3, R_c = 3.91 \times 10^6$, and $\alpha = 12$ deg.

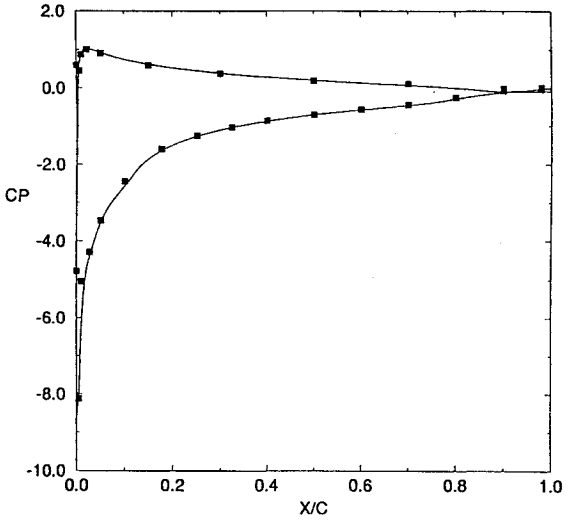

Fig. 15 Comparison of calculated (solid lines) and measured (symbols) pressure coefficient distributions with the full-potential method for the NLR-1 airfoil at $M_\infty = 0.3, R_c = 3.91 \times 10^6$, and $\alpha = 12$ deg.

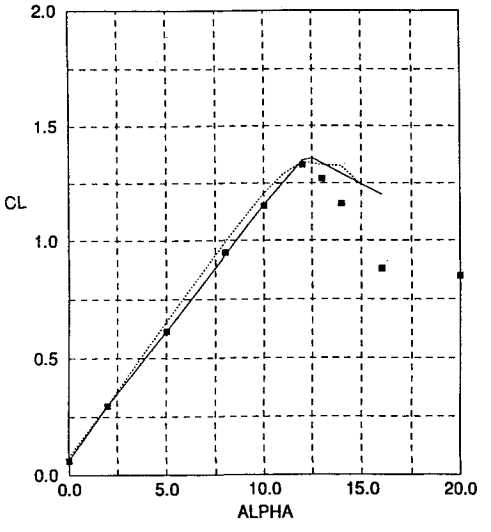

Fig. 16 Comparison of calculated and measured lift coefficients for the NLR-1 airfoil at $M_\infty = 0.3$ and $R_c = 3.91 \times 10^6$. Solid lines denote the results with the full-potential method and dashed lines those with the modified panel method.

shows a comparison between measured and calculated lift coefficients. For this airfoil, the predicted $(C_\ell)_{max}$ with the modified panel method is in good agreement with the predicted $(C_\ell)_{max}$ with the full-potential method, as well as with the experimental value; surprisingly enough, however, the predicted lift coefficients with the modified panel method are not in as good agreement with the measurements at lower angles of attack than they are at the stall angles, whereas those predicted with the full-potential method are in excellent agreement with data.

IV. Concluding Remarks

The results and discussion of the previous section and those in Ref. 18 show that the present interactive boundary-layer and stability and transition method combined with an improved turbulence model and with a full-potential method, leads to values of lift coefficients that are in very good agreement with experiment for compressible flows at low freestream Mach numbers. The panel method used for inviscid flows with viscous effects shows good agreement with data for incompressible flows but is not satisfactory for compressible flows at low Mach number flows with compressibility corrections.

The calculations also indicate the important role of the Reynolds number at low Reynolds numbers. The presence of rather extensive separation bubbles even at low angles of attack requires the transition calculations to be performed interactively.

Acknowledgments

This work was supported by the Air Force Office of Scientific Research (AFOSR) under Contract AFOSR 90-0262 and under NASA RFR-0352. The authors would like to thank D. Fant for the AFOSR support.

References

[1]Michel, R., "Etude de la Transition sur les Profiles d'Aile; Establishment d'un Critere de Determination de Point de Transition et Calcul de la Trainee de Profile Incompressible, ONERA Rept. 1/1578A, 1951.

[2]Granvillle, P. S., "The Calculation of the Viscous Drag of Bodies of Revolution," David W. Taylor Model Basin, Rept. 849, 1953.

[3]Smith, A. M. O., "Transition, Pressure Gradient, and Stability Theory," *Proceedings of the IX International Congress of Applied Mechanics* (Brussels, Belgium), Vol. 4, 1956, pp. 234–244.

[4]Van Ingen, J. L., "A Suggested Semi-Empirical Method for the Calculation of the Boundary-Layer Region," Rept. VTH71, VTH74, Delft, Holland, 1956.

[5]Cebeci, T., and Smith, A. M. O., *Analysis of Turbulent Boundary Layers*, Academic Press, New York, 1974.

[6]Dhawan, S., and Narasimha, R., "Some Properties of Boundary-Layer Flow During the Transition from Laminar to Turbulent Motion," *Journal of Fluid Mechanics*, Vol. 3, 1958, pp. 418–436.

[7]Chen, K. K., and Thyson, N. A., "Extension of Emmons' Spot Theory to Flows on Blunt Bodies, " *AIAA Journal*, Vol. 9, 1971, pp. 821–825.

[8]Cebeci, T., Clark, R. W., Chang, K. C., Halsey, N. D., and Lee, K., "Airfoils with Seperation and the Resulting Wakes," *Journal of Fluid Mechanics*, Vol. 163, 1986, pp. 323–347.

[9]Cebeci, T., Jau, J., Vitiello, D., and Chang, K. C., "Prediction of Post-Stall Flows on Airfoils," *Numerical and Physical Aspects of Aerodynamic Flows IV*, edited by T. Cebeci, Springer-Verlag, Heidelberg, Germany, 1990, pp. 93–106.

[10]Gleyzes, C., Cousteix, J., and Bonnet, J. L., "A Calculation Method of Leading-Edge Separation Bubbles," *Numerical and Physical Aspects of Aerodynamic Flows II*, edited by T. Cebeci, Springer-Verlag, New York, 1984, pp. 173–192.

[11]Drela, M., and Giles, M. B., "Viscous-Inviscid Analysis of Transonic and Low Reynolds Number Airfoils," *AIAA Journal*, Vol. 25, No. 10, 1987, pp. 1347–1355.

[12]Walker, G. J., Subroto, P. H., and Platzer, M. F., "Transition Modeling Effects on Viscous/Inviscid Interaction Analysis of Low Reynolds Number Airfoil Flows Involving Laminar Separation Bubbles," American Society of Mechanical Engineers, ASME Paper 88-GT-32, June 1988.

[13]Cebeci, T., "Essential Ingredients of a Method for Low Reynolds-Number Airfoil," *AIAA Journal*, Vol. 27, 1989, p. 1680.

[14]Hess, J. L., and Smith, A. M. O., "Calculation of Potential Flow About Arbitrary Bodies," *Progress in Aerospace Sciences*, Vol. 8, Pergamon, New York, 1966.

[15]Bharadvaj, B. K., "Computational of Steady and Unsteady Control Surface Loads in Transonic Flow," *AIAA Journal*, Vol. 29, No. 11, 1991, pp. 1906–1922.

[16]Cebeci, T., Roknaldin, F., and Carr, L. W., "Prediction of Stall and Post-Stall Behavior of Airfoils at Low and High Reynolds Numbers," AIAA Paper 93-3502, Jan. 1993.

[17]Carr, L. W., McCroskey, W. J., McAlister, K. W., Pucci, S. L., and Lambert, O., "An Experimental Study of Dynamic Stall on Advanced Airfoil Sections, Vol. 3, Hot-Wire and Hot-Film Measurements," NASA TM 84245.

[18]Cebeci, T., and Carr, L. W., "Calculation of the Stall and Post-Stall Behavior of Airfoils at Low Mach Numbers," NASA Rept. (in preparation).

[19]Chen, H. H., and Cebeci, T., "The Role of Separation Bubbles on the Aerodynamic Characteristics of Airfoils, Including Stall at Low Reynolds Numbers" (paper in review).

[20]McGhee, R. J., Jones, G. S., and Jouty, R., "Performance Characteristics from Wind-Tunnel Tests of a Low Reynolds-Number Airfoil," AIAA Paper 88-0607, Jan. 1988.

[21]Hicks, R. M., and McCroskey, W. J., "An Experimental Evaluation of a Helicopter Rotor Section Design by Numerical Optimization," NASA TM-78622, 1980.

[22]Wortmann, F. X., "Design of Airfoils with High Lift at Low and Medium Subsonic Mach Numbers," AGARD Conference Proceedings CP-102, Advisory Group for Aerospace Research and Development, Paper 7, Neuilly-sur-Seine, France, 1972.

[23]Dadone, L. U., "Two-Dimensional Wind Tunnel Test of an Oscillating Rotor Airfoil Volume 1," NASA CR 2914, 1977.